Infectious Disease Modelling 6 (2021) 729–742

Contents lists available at ScienceDirect

Infectious Disease Modelling

journal homepage: www.keaipublishing.com/idm

Social distancing and testing as optimal strategies against the spread of COVID-19 in the Rio Grande Valley of Texas

Kristina P. Vatcheva [a, *], Josef Sifuentes [b], Tamer Oraby [b], Jose Campo Maldonado [c], Timothy Huber [b], María Cristina Villalobos [b]

[a] School of Mathematical & Statistical Sciences, University of Texas Rio Grande Valley, Brownsville, TX, 78520, USA
[b] School of Mathematical & Statistical Sciences, University of Texas Rio Grande Valley, Edinburg, TX, 78539, USA
[c] School of Medicine, The University of Texas Rio Grande Valley, Edinburg, TX, 78539, USA

ARTICLE INFO

Article history:
Received 19 October 2020
Received in revised form 12 April 2021
Accepted 13 April 2021
Available online 24 April 2021
Handling editor: Dr HE DAIHAI HE

Keywords:
COVID-19
Mathematical modeling
Optimal control
Rio Grande Valley (RGV)
Testing and social distancing
School reopening

ABSTRACT

At the beginning of August 2020, the Rio Grande Valley (RGV) of Texas experienced a rapid increase of coronavirus disease 2019 (abbreviated as COVID-19) cases and deaths. This study aims to determine the optimal levels of effective social distancing and testing to slow the virus spread at the outset of the pandemic. We use an age-stratified eight compartment epidemiological model to depict COVID-19 transmission in the community and within households. With a simulated 120-day outbreak period data we obtain a post 180-days period optimal control strategy solution. Our results show that easing social distancing between adults by the end of the 180-day period requires very strict testing a month later and then daily testing rates of 5% followed by isolation of positive cases. Relaxing social distancing rates in adults from 50% to 25% requires both children and seniors to maintain social distancing rates of 50% for nearly the entire period while maintaining maximum testing rates of children and seniors for 150 of the 180 days considered in this model. Children have higher contact rates which leads to transmission based on our model, emphasizing the need for caution when considering school reopenings.

1. Introduction

An outbreak of coronavirus disease 2019 (COVID-19) caused by a novel severe acute respiratory syndrome coronavirus 2 (SARS-CoV-2) was documented in Wuhan, Hubei Province, China in December 2019 (World Health Organization, 2020). By March 11, 2020, COVID-19 had been declared a pandemic by the World Health Organization (WHO) (World Health Organization, 2020a) and is currently affecting almost every territory and country in the world (World Health Organization, 2020b) resulting in more than 120 million COVID-19 confirmed cases and 2.7 million deaths (World Health Organization, 2020b) as of March 15, 2021. COVID-19 activity in the United States (U.S.) has been heterogeneous with broad regional variation and more than 29.5 million cases and over 535,000 deaths as of March 15, 2021 (Dong, Du, &

* Corresponding author. School of Mathematical & Statistical Sciences, University of Texas Rio Grande Valley, One West University Blvd., Brownsville, TX, 78520, USA.
E-mail address: Kristina.Vatcheva@utrgv.edu (K.P. Vatcheva).
Peer review under responsibility of KeAi Communications Co., Ltd.

https://doi.org/10.1016/j.idm.2021.04.004

Gardner, 2020). The duration and severity of each pandemic interval can vary depending on the characteristics of the outbreak and the public health response (Centers for Disease Control and Prevention, 2021). Early in the COVID-19 pandemic across the world an exponential growth trajectory was reported (Sanche et al., 2020; Yuan, Li, Lv, & Lu, 2020). In that case, the rate of the spread of the infection was proportional to the number of people infected.

COVID-19 transmits predominantly through respiratory droplets produced when an infected person coughs or sneezes and possibly through very small, aerosolized particles and by contaminated surface contact (Centers for Disease Control and Prevention, 2021a). The Centers for Disease Control and Prevention (CDC) provided guiding principles regarding the Implementation of Mitigation Strategies for Communities with local COVID-19 transmissions, including limiting community movement and school and work closures in the setting of substantial or widespread community transmission; these guiding principles are frequently updated based on the status of the community (Centers for Disease Control and Prevention, 2021a). COVID-19 vaccine distribution began in the U.S. on December 14, 2020 and as of March 15, 2021 only 21.4% of the total U.S. population had been vaccinated (NPR, 2021). Strategies, efficiency, and equity of the distribution vary from state to state (NPR, 2021). The CDC and public health experts continue to recommend the public to practice social distancing, hand washing, cough etiquette, and wearing a mask covering the mouth and nose as more is understood about how COVID-19 vaccines work in real-world conditions (Centers for Disease Control and Prevention, 2021; Centers for Disease Control and Prevention, 2021a).

Studies have shown that school closures, workplace dismissal, reduced community contact, stay-at-home orders, and isolation of symptomatic individuals will delay and reduce the peak attack rate; thus diminishing pressure on health services, and reducing mortality of respiratory infections (Bolton et al., 2012; Chowell et al., 2011; Herrera-Valdez, Cruz-Aponte, & Castillo-Chavez, 2011; Kelso, Milne, & Kelly, 2009; Koo et al., 2020; Nasrullah et al., 2012; Shim, 2013). A mathematical modeling study conducted in Singapore confirms that implementing the combined intervention of isolating infected individuals and quarantining their family members, workplace distancing, and school closures could substantially reduce the number of COVID-19 infections (Koo et al., 2020).

Apart from the coordinated and consistent stay-at-home orders, rapid increase of SARS-CoV-2 testing is also one of the tools implemented to respond to the COVID-19 pandemic (Guest, Del Rio, & Sanchez, 2020). Broader and faster turnaround testing can improve our understanding of the outbreak and inform modeling and analysis decision making. In Iceland, testing of individuals suspected of having COVID-19 and those who are asymptomatic showed that of those infected, approximately 50% were asymptomatic according to early reports (The Week, 2020). Recent studies indicate that pre-symptomatic and asymptomatic transmission likely play a significant role in the spread of COVID-19 (Pan et al., 2020; Tong et al., 2020; World Health Organization, 2020b) and estimate the prevalence of asymptomatic SARS-CoV-2 in the range of 40%–45% (Oran & Topol, 2020). By using a broad testing strategy, Germany was able to trace and rapidly identify cases of COVID-19 resulting in early isolation of infected individuals, preparedness of the hospital system, and low fatality rates (The Conversation, 2020).

The Rio Grande Valley (RGV) includes four Texas counties located along the U.S.-Mexico border: Starr County, Hidalgo County, Willacy County, and Cameron County. The first case in RGV was reported in Cameron County on March 19, 2020 followed by Hidalgo on March 21 and Willacy and Starr County on March 26 (KVEO-TV, 2020). Most of the initial cases were travel related (KVEO-TV, 2020). Strict rules, such as travel restrictions and shelter in place orders were implemented across the RGV in an effort to stop the spread of the disease (FOX News San Antonio, 2020). As the first phase of reopening Texas started on May 1, 2020, the number of confirmed COVID-19 cases in the RGV increased from 768 to 55,740 at the beginning of August 2020, and 100,617 cases on March 15, 2021; and the number of reported deaths increased from 25 to 2373 at the beginning of August 2020, to 4159 on March 15, 2021 (Texas Health and Human Services. Texas Department of State Health Services, 2021).

According to the U.S. Census Bureau, the estimated RGV population was 1,305,782 with more than 90% of the population as Hispanic or Latino on July 1, 2019 (The United States Census Bureau, 2020). Several studies have characterized the Mexican American population living in this region as having high poverty rates, low educational attainment, low health literacy, lack of health care coverage, extremely high rates of obesity, type 2 diabetes, metabolic complications, cardiovascular diseases and other diseases (Laing et al., 2015; Vatcheva, Fisher-Hoch, Reininger, & McCormick, 2020).

Based on currently available information and clinical expertise on COVID-19, the CDC warns that older adults and people of any age who have serious underlying medical conditions, such as chronic lung disease or moderate to severe asthma, diabetes, severe obesity, liver disease, serious heart conditions, and chronic kidney disease might be at higher risk for severe illness resulting from COVID-19 (Centers for Disease Control and Prevention, 2021b). Therefore, optimal COVID-19 prevention strategies are crucial everywhere, but especially for the RGV population.

Various deterministic compartmental (SEIR) models have been proposed to describe the COVID-19 transmission dynamic and to examine the effectiveness of current strategies to face the COVID-19 outbreak (Kim, Kim, Peck, & Jung, 2020; Pasco et al., 2020; Wan et al., 2020; Weissman et al., 2020). These models include non-pharmaceutical interventions (NPI) to control the coronavirus disease by slowing its spread and are used to predict hospital capacity needs. Some of those mathematical models did not incorporate the rapidly evolving understanding of COVID-19 underreporting and the likely significant role of pre-symptomatic and asymptomatic transmissions of COVID-19.

In this study we use an optimal control approach in a deterministic epidemiological model to depict the COVID-19 outbreak in the RGV. The model is comprised of a system of ordinary differential equations to model the transmission of the virus between three age groups in the community and within households and the transitions of infected individuals between the different compartments. Optimal control is a powerful optimization technique to determine the appropriate

levels of effective interventions required to slow viral transmission, including social distancing and the extent of testing needed. These optimal strategies could assist in determining the feasibility of return to work and school reopenings.

2. Methods

2.1. Deterministic model description

We use a deterministic epidemiological model to depict COVID-19 transmission in the community and within households (Fig. 1). The model is comprised from the following eight compartments: susceptible ($\boldsymbol{S}$); exposed ($\boldsymbol{E}$); infected but asymptomatic ($\boldsymbol{I^A}$); mildly infected and symptomatic ($\boldsymbol{I^M}$); severely infected, symptomatic, and hospitalized ($\boldsymbol{I^H}$); confirmed infected and isolated at home ($\boldsymbol{Q}$); recovered/removed ($\boldsymbol{R}$); and dead ($\boldsymbol{D}$). We assume that all severely infected individuals get hospitalized and that exposed individuals do not transmit the disease until they move out of compartment $\boldsymbol{E}$. We classify individuals by one of the three age groups: children (0–18 years), denoted by subscript c; adults (19–64 years) denoted by subscript a; and seniors (65 years or older) denoted by subscript s. The subpopulation sizes are denoted by $\boldsymbol{N_c}$, $\boldsymbol{N_a}$, and $\boldsymbol{N_s}$, respectively, and they add up to the total population size $\boldsymbol{N}$. We assume an initial number of individuals in the compartments $\boldsymbol{S}, \boldsymbol{E}, \boldsymbol{I^A}, \boldsymbol{I^M}$, and $\boldsymbol{I^H}$ which are provided in Table 1.

The age-stratified mathematical model to depict the dynamics of disease transmission is provided with the following system of ordinary differential equations that incorporate the time-dependent age-stratified control functions $\boldsymbol{\rho_j}(\boldsymbol{t})$ (in the definition of $\boldsymbol{\pi_j}$)and $\boldsymbol{\delta_j}(\boldsymbol{t})$:

$$\frac{\mathbf{dS_j}}{\mathbf{dt}} = -\boldsymbol{\pi}_\mathbf{j}\, \boldsymbol{S}_\mathbf{j} \tag{1}$$

$$\frac{\mathbf{dE_j}}{\mathbf{dt}} = \boldsymbol{\pi}_\mathbf{j}\, \boldsymbol{S}_\mathbf{j} - \alpha\, \boldsymbol{E}_\mathbf{j} \tag{2}$$

$$\frac{\mathbf{dI_j^A}}{\mathbf{dt}} = \alpha(\mathbf{1}-\mathbf{p})\boldsymbol{E}_\mathbf{j} - \mu_\mathbf{A}\boldsymbol{I}_\mathbf{j}^\mathbf{A} - \delta_\mathbf{j}\boldsymbol{I}_\mathbf{j}^\mathbf{A} \tag{3}$$

$$\frac{\mathbf{dI_j^M}}{\mathbf{dt}} = \alpha\boldsymbol{p}\boldsymbol{E}_\mathbf{j} - (\mu_\mathbf{M} + \gamma + \mathbf{q})\boldsymbol{I}_\mathbf{j}^\mathbf{M} \tag{4}$$

$$\frac{\mathbf{dI_j^H}}{\mathbf{dt}} = \gamma\boldsymbol{I}_\mathbf{j}^\mathbf{M} + \nu_\mathbf{Q}\mathbf{Q_j} - (\mu_\mathbf{H} + \sigma_\mathbf{j})\boldsymbol{I}_\mathbf{j}^\mathbf{H} \tag{5}$$

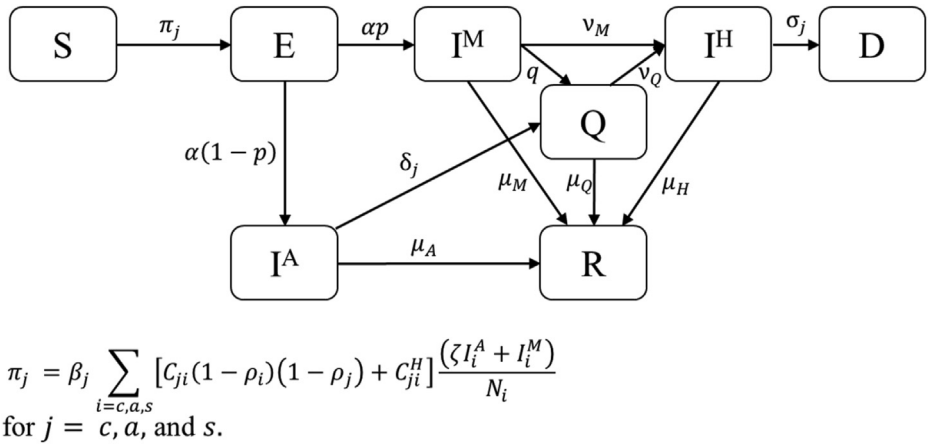

$$\pi_j = \beta_j \sum_{i=c,a,s} \left[C_{ji}(1-\rho_i)(1-\rho_j) + C_{ji}^H\right]\frac{\left(\zeta I_i^A + I_i^M\right)}{N_i}$$
$$\text{for } j = c, a, \text{and } s.$$

Fig. 1. Deterministic epidemiological model to depict COVID-19 transmission between compartments in the Rio Grande Valley, Texas. The compartments are: susceptible ($\boldsymbol{S}$); exposed ($\boldsymbol{E}$); infected but asymptomatic ($\boldsymbol{I^A}$); mildly infected and symptomatic ($\boldsymbol{I^M}$); severely infected, symptomatic, and hospitalized ($\boldsymbol{I^H}$); detected infections and isolated at home ($\boldsymbol{Q}$); recovered/removed ($\boldsymbol{R}$); and dead ($\boldsymbol{D}$).

Table 1
Definition of parameters and baseline values used in the mathematical model.

Parameters or variables	Description	Base value	Source/Reference
	Demographic		
N_c	Children population (0–18 y) size	437,722	The United States Census Bureau (2020)
N_a	Adult population (19–64 y) size	776,293	The United States Census Bureau (2020)
N_s	Senior population (65+ y) size	163,848	The United States Census Bureau (2020)
	Disease-specific		
β_c	Children infection probability upon contact with an infectious individual	$\beta_c = 0.2287$	Based on calibration
β_a	Adult infection probability upon contact with an infectious individual	$\beta_a = 0.0396$	Based on calibration
β_s	Senior infection probability upon contact with an infectious individual	$\beta_s = 0.4994$	Based on calibration
α	Rate of removal from exposed compartment (per day) (reciprocal of incubation period)	$\alpha = \frac{1}{5.1}$	Lauer et al., 2020; Linton et al. (2020)
ζ	Scale parameter for infected asymptomatic (I^A)	$\zeta = 1$	Assumption based on worst case asymptomatic infectiousness
p	Probability of showing symptoms among those exiting the exposed compartment	$p = 74\%$	The New York Times (2020)
ν_M	Rate of progression from mild to severe infection	$\nu_M = \frac{1}{14}$	World Health Organization (2020c)
μ_A	Recovery rate of asymptomatic	$\mu_A = \frac{1}{7}$	Assumption
μ_M	Recovery rate of mildly infected	$\mu_M = \frac{1}{12}$	Assumption
μ_H	Recovery rate for severely infected and hospitalized	$\mu_H = \frac{1}{31.5}$	G. Huang et al., 2020; World Health Organization, 2020c
γ	The rate of hospitalization of mildly infected	$\gamma = 0.0071$	Based on calibration
μ_Q	Recovery rate of quarantined	$\mu_Q = (\mu_M^{-1} - q^{-1})^{-1}$	–
ν_Q	Hospitalization rate of originally quarantined individuals	$\nu_Q = (\gamma^{-1} - q^{-1})^{-1}$	–
σ_j	Disease-specific death rate for children (c), adults (a), and seniors (s) for $j \in \{c, a, s\}$	(j0.0%, 0.6%, 4.6%)	CDC COVID-19 Response Team (2020)
	Social and Household		
C	Social contact matrix (rates per day)	$\begin{pmatrix} 3.6995 & 3.6995 & 0.1356 \\ 1.1996 & 7.1355 & 0.0928 \\ 0.1642 & 0.8274 & 0.1483 \\ 2.4113 & 2.3297 & 0.0550 \end{pmatrix}$	Prem, Cook, and Jit (2017)
C^H	Household contact matrix (rates per day)	$\frac{1}{5}\begin{pmatrix} 1.9084 & 1.7166 & 0.0623 \\ 1.5759 & 1.4757 & 0.2529 \end{pmatrix}$	Prem et al. (2017)
	Interventions		
ρ_j	Initial proportion of individuals practicing social distancing prior to optimal control analysis for $j \in \{c, a, s\}$	$\rho_{c,a,s} = (0.36, 0.36, 0.36)$	Based on calibration
$[t_{0,i}, t_{1,i}]$	Beginning and end times of social distancing for the three age groups for $i = \{c, a, s\}$	[0, 120] days	Assumption
q	Probability of quarantine	60%	CDC, 2021b
δ_j	Initial testing rates prior to optimal control analysis for $j \in \{c, a, s\}$	$\delta_{c,a,s} = (0.02, 0.02, 0.02)$	

$$\frac{dQ_j}{dt} = qI_j^M + \delta_j I_j^A - (\mu_Q + \nu_Q)Q_j \tag{6}$$

$$\frac{dR_j}{dt} = \mu_A I_j^A + \mu_M I_j^M + \mu_H I_j^H + \mu_Q Q_j \tag{7}$$

$$\frac{dD_j}{dt} = \sigma_j I_j^H \tag{8}$$

where $j \in \{c, a, s\}$ is the subscript for age.

Note that we are making the simplifying assumption that N_j is constant given that our model only considers a relatively short span of time of 180 days and thus, we define N_j as follows

$$N_j(t) = S_j(t) + E_j(t) + I_j^A(t) + I_j^M(t) + I_j^H(t) + Q_j(t) + R_j(T)$$

for $j \in \{c, a, s\}$

The social contact matrix C defines the contact rates between the three age groups

$$C = \begin{pmatrix} C_{cc} & C_{ca} & C_{cs} \\ C_{ac} & C_{aa} & C_{as} \\ C_{sc} & C_{sa} & C_{ss} \end{pmatrix}, \tag{10}$$

and the household contact matrix C^H defines the contact rates between the three age groups

$$C^H = \begin{pmatrix} C^H_{cc} & C^H_{ca} & C^H_{cs} \\ C^H_{ac} & C^H_{aa} & C^H_{as} \\ C^H_{sc} & C^H_{sa} & C^H_{ss} \end{pmatrix} \tag{11}$$

Their values are provided in Table 1.

Furthermore, notice that in equations (1) and (2) the social distancing control ρ_j appears quadratically. This is due to the fact that the social distancing control is prescribed to the susceptible, asymptomatic and mildly infected groups alike. The interactions amongst these groups in the same age bracket are responsible for the quadratic terms.

While the inclusion of these quadratic control terms adds computational complexity to the optimal control model and algorithm, it is necessary to more accurately model an epidemic that is driven largely by asymptomatic and mildly infected carriers of the virus. Other papers model this dynamic linearly (Perkins & España, 2020; Tsay, Lejarza, Stadtherr, & Baldea, 2020).

For simplicity, we write equations (1) − (8) as

$$\dot{x} = f(t, x, u)$$

where $x = [S_j, E_j, I^A_j, I^M_j, I^H_j, Q_j, R_j, D_j; j \in \{c, a, s\}]^T$ and $u = [\rho_j, \delta_j; j \in \{c, a, s\}]^T$.

2.2. Objective functional

The optimal control problem has the state equations (1) − (8) with objective functional

$$F(u) = \int_0^T \sum_{j \in \{a,\, c,\, s\}} \left\{ C^\rho_j \rho^2_j(t) \left[S_j(t) + E_j(t) + I^A_j(t) \right] + C_T \delta^2_j(t) N_j(t) + C_H I^H_j(t) \right\} dt \tag{12}$$

where $\rho_j(t) \in [0,\ 1]$ and $\delta_j(t) \in [0, 0.1]$ are the six control variables. The control variable $\rho_j(t)$ describes the proportion of social distancing among the three different age groups in compartments S, E, and I^A. The control variable $\delta_j(t)$ describes the proportion of individuals per day to test among the three different age groups to determine which individuals to isolate. The parameters C^ρ_j are the cost per day associated with the social distancing of group j; C_T is the cost per test (which can be interpreted as per person); and C_H is the cost associated with hospitalization per person per day. The time interval $[0,\ T]$ is given in terms of days where T is the final time described as 180 days. The cost parameters do not represent cost in dollars, but penalty terms, or weights meant to model the costs to the population assessed in this paper (Lenhart, S., Workman, J.T., 2007). The values of the cost parameters used in our study are given below:

$$C^\rho_c = 10,\ C^\rho_a = 50,\ C^\rho_s = 10;\ C_T = 100,\ C_H = 13,000.$$

The C^ρ_j values represent the cost of social distancing which is weighed five times as much for adults as children and seniors. Since we are using a well-mixed differential equation model, these values are meant to model average values, while some adults may pay little cost to work from home and with this to maintain social distancing, others incur substantial costs from social distancing. The cost of testing, which would include the cost of the test itself as well as the logistics for distributing, administering and carrying out tests, was set as two days cost of an adult social distancing. The most substantial cost is the cost of hospitalization. The daily cost of a hospitalization can vary dramatically for different patients based on what procedures and interventions are required and level of health insurance. This cost can also be considered as a knob used to dampen the infection incidence rates when optimally controlled.

Hence the goal is to minimize the cost due to social distancing, hospitalization, and testing. In summary, the optimal control problem becomes

$\min_u F(u)$ subject to $\dot{x} = f(t, x, u)$.

2.3. Optimality conditions

In this section, we apply Pontryagin's maximum principle to describe the first-order necessary conditions for the optimal control problem with objective functional (12)

$\min_u F(u)$ subject to $\dot{x} = f(t, x, u)$.

To apply Pontryagin's maximum principle, we first define the Hamiltonian of the optimal control problem as

$$\boldsymbol{H}(\mathbf{x},\ \lambda,\ \boldsymbol{u}) = \sum_{\boldsymbol{j}\in\{\boldsymbol{a},\ \boldsymbol{c},\ \boldsymbol{s}\}} \left\{ \boldsymbol{C}_{\boldsymbol{j}}^{\rho}\rho_{\boldsymbol{j}}^{2}(\boldsymbol{t})\left[\ \boldsymbol{S}_{\boldsymbol{j}}(\boldsymbol{t}) + \boldsymbol{E}_{\boldsymbol{j}}(\boldsymbol{t}) + \boldsymbol{I}_{\boldsymbol{j}}^{\boldsymbol{A}}(\boldsymbol{t})\right] + \boldsymbol{C}_{\boldsymbol{T}}\delta_{\boldsymbol{j}}^{2}(\boldsymbol{t})\boldsymbol{N}_{\boldsymbol{j}}(\boldsymbol{t}) + \boldsymbol{C}_{\boldsymbol{H}}\boldsymbol{I}_{\boldsymbol{j}}^{\boldsymbol{H}}(\boldsymbol{t})\right\} \ +\ \lambda^{\boldsymbol{T}}\mathbf{f}(\boldsymbol{t},\mathbf{x},\boldsymbol{u}) \tag{13}$$

where $\lambda \equiv \lambda(\boldsymbol{t}) = [\lambda_{\boldsymbol{S}_j}(\boldsymbol{t}), \lambda_{\boldsymbol{E}_j}(\boldsymbol{t}), \lambda_{\boldsymbol{I}_j^A}(\boldsymbol{t}), \lambda_{\boldsymbol{I}_j^M}(\boldsymbol{t}), \lambda_{\boldsymbol{I}_j^H}(\boldsymbol{t}), \lambda_{\boldsymbol{Q}_j}(\boldsymbol{t})]^{\boldsymbol{T}}$ for $\boldsymbol{j}\in\{\boldsymbol{c},\boldsymbol{a},\boldsymbol{s}\}$ is the vector of adjoint variables. Letting $\boldsymbol{H} = \boldsymbol{H}(\mathbf{x},\lambda,\boldsymbol{u})$ and expanding the right-most term in the Hamiltonian, we describe the Hamiltonian explicitly as

$$\begin{aligned}
H \ =\ & \sum_{\boldsymbol{j}}\left\{ \boldsymbol{C}_{\boldsymbol{j}}^{\rho}\rho_{\boldsymbol{j}}^{2}(\boldsymbol{t})\left[\ \boldsymbol{S}_{\boldsymbol{j}}(\boldsymbol{t}) + \boldsymbol{E}_{\boldsymbol{j}}(\boldsymbol{t}) + \boldsymbol{I}_{\boldsymbol{j}}^{\boldsymbol{A}}(\boldsymbol{t})\right] + \boldsymbol{C}_{\boldsymbol{T}}\delta_{\boldsymbol{j}}^{2}(\boldsymbol{t})\boldsymbol{N}_{\boldsymbol{j}}(\boldsymbol{t}) + \boldsymbol{C}_{\boldsymbol{H}}\boldsymbol{I}_{\boldsymbol{j}}^{\boldsymbol{H}}\right\} \\
& + \sum_{\boldsymbol{j}}\lambda_{\boldsymbol{S}_j}(\boldsymbol{t})\ \{\ -\pi_{\boldsymbol{j}}\boldsymbol{S}_{\boldsymbol{j}}\} \\
& + \sum_{\boldsymbol{j}}\lambda_{\boldsymbol{E}_j}(\boldsymbol{t})\ \{\pi_{\boldsymbol{j}}\boldsymbol{S}_{\boldsymbol{j}} - \alpha\boldsymbol{E}_{\boldsymbol{j}}\} \\
& + \sum_{\boldsymbol{j}}\lambda_{\boldsymbol{I}_j^A}^{A}(\boldsymbol{t})\left\{\alpha(1-\boldsymbol{p})\boldsymbol{E}_{\boldsymbol{j}} - \mu_{\boldsymbol{A}}\boldsymbol{I}_{\boldsymbol{j}}^{\boldsymbol{A}} -\ \delta_{\boldsymbol{j}}\boldsymbol{I}_{\boldsymbol{j}}^{\boldsymbol{A}}\right\} \\
& + \sum_{\boldsymbol{j}}\lambda_{\boldsymbol{I}_{\boldsymbol{j}}^{\boldsymbol{M}}}(\boldsymbol{t})\left\{\alpha\boldsymbol{p}\boldsymbol{E}_{\boldsymbol{j}} - (\mu_{\boldsymbol{M}} + \gamma + \boldsymbol{q})\boldsymbol{I}_{\boldsymbol{j}}^{\boldsymbol{M}}\right\} \\
& + \sum_{\boldsymbol{j}}\lambda_{\boldsymbol{I}_{\boldsymbol{j}}^{\boldsymbol{H}}}(\boldsymbol{t})\left\{\gamma\boldsymbol{I}_{\boldsymbol{j}}^{\boldsymbol{M}} +\ \nu_{\boldsymbol{Q}}\boldsymbol{Q}_{\boldsymbol{j}} - (\mu_{\boldsymbol{H}} + \sigma_{\boldsymbol{j}})\boldsymbol{I}_{\boldsymbol{j}}^{\boldsymbol{H}}\right\} \\
& + \sum_{\boldsymbol{j}}\lambda_{\boldsymbol{Q}_j}\left\{\boldsymbol{q}\boldsymbol{I}_{\boldsymbol{j}}^{\boldsymbol{M}} + \delta_{\boldsymbol{j}}\boldsymbol{I}_{\boldsymbol{j}}^{\boldsymbol{A}} - (\mu_{\boldsymbol{Q}} + \nu_{\boldsymbol{Q}})\boldsymbol{Q}_{\boldsymbol{j}}\right\}.
\end{aligned} \tag{14}$$

The necessary conditions that the optimal control $\boldsymbol{u}^*(\boldsymbol{t}) = [\rho_{\boldsymbol{j}}^*(\boldsymbol{t}), \delta_{\boldsymbol{j}}^*(\boldsymbol{t})]$ for $\boldsymbol{j}\in\{\boldsymbol{c},\boldsymbol{a},\boldsymbol{s}\}$ and state variable x^* must satisfy are the following:

$$\lambda'(\boldsymbol{t}) = -\frac{\partial \boldsymbol{H}}{\partial \mathbf{x}} \qquad \textit{Adjoint equation} \tag{15}$$

$$\lambda\left(\boldsymbol{t}_{\boldsymbol{f}}\right) = 0 \qquad \textit{Transversality condition} \tag{16}$$

$$\frac{\partial\, \boldsymbol{H}(\boldsymbol{u}^*)}{\partial \boldsymbol{u}} = 0 \qquad \textit{Optimality condition} \tag{17}$$

$$\dot{\mathrm{x}} = \mathrm{f}(\boldsymbol{t}, \mathrm{x}^*, \boldsymbol{u}^*) \qquad \textit{ODE system.}$$

The adjoint equations for $\boldsymbol{j}\in\{\boldsymbol{c},\boldsymbol{a},\boldsymbol{s}\}$ are given in the Appendix. Expanding on the transversality condition above we obtain

$$\lambda_{\boldsymbol{S}_j}\left(\boldsymbol{t}_{\boldsymbol{f}}\right) = 0 \quad \lambda_{\boldsymbol{I}_{\boldsymbol{j}}^{\boldsymbol{M}}}\left(\boldsymbol{t}_{\boldsymbol{f}}\right) = 0$$

$$\lambda_{\boldsymbol{E}_j}\left(\boldsymbol{t}_{\boldsymbol{f}}\right) = 0 \quad \lambda_{\boldsymbol{I}_{\boldsymbol{j}}^{\boldsymbol{H}}}\left(\boldsymbol{t}_{\boldsymbol{f}}\right) = 0 \quad \text{for } j\in\{c,a,s\}$$

$$\lambda_{\boldsymbol{I}_{\boldsymbol{j}}^{\boldsymbol{A}}}\left(\boldsymbol{t}_{\boldsymbol{f}}\right) = 0 \quad \lambda_{\boldsymbol{Q}_j}\left(\boldsymbol{t}_{\boldsymbol{f}}\right) = 0.$$

Finally, the optimality condition $\frac{\partial \boldsymbol{H}(\boldsymbol{u}^*)}{\partial \boldsymbol{u}} = 0$ provides the characterization for the optimal control $\boldsymbol{u}^* = [\,\rho_{\boldsymbol{k}}^*(\boldsymbol{t}), \delta_{\boldsymbol{k}}^*(\boldsymbol{t})]$ for $\boldsymbol{k}\in\{\boldsymbol{c},\boldsymbol{a},\boldsymbol{s}\}$ and $0 \le \boldsymbol{p}_{\boldsymbol{k}}(\boldsymbol{t}) \le 1$ and $0 \le \boldsymbol{\delta}_{\boldsymbol{k}}(\boldsymbol{t}) \le 0.1$ which are given by

$$\rho_{\boldsymbol{k}}^*(\boldsymbol{t}) = \min\left\{1, \max\left\{0, \frac{\boldsymbol{A}_{\boldsymbol{k}}(\boldsymbol{t})}{\boldsymbol{B}_{\boldsymbol{k}}(\boldsymbol{t})}\ \right\}\right\}$$

where $\boldsymbol{G}_{\boldsymbol{i}} = \frac{\zeta\, \boldsymbol{I}_{\boldsymbol{i}}^{\boldsymbol{A}} + \boldsymbol{I}_{\boldsymbol{i}}^{\boldsymbol{M}}}{\boldsymbol{N}_{\boldsymbol{i}}}$ for $\boldsymbol{i}\in\{\boldsymbol{c},\boldsymbol{a},\boldsymbol{s}\}$ and

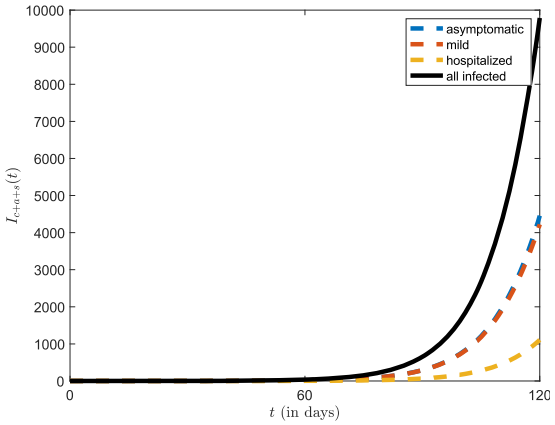

Fig. 2. Total infection incidence rates, total asymptomatic cases, total mild cases, and total hospitalization rates for 120-day period from February 27, 2020 to June 26, 2020 in the Rio Grande Valley, Texas.

$$\boldsymbol{A_k(t)} = \sum_{\boldsymbol{j\neq k}} \boldsymbol{S_j}\left(\lambda_{\boldsymbol{E_j}} - \lambda_{\boldsymbol{S_j}}\right)\left(\boldsymbol{\beta_j}(1-\boldsymbol{\rho_j})\boldsymbol{C_{jk}}\boldsymbol{G_k}\right) +$$

$$\boldsymbol{S_k}\left(\lambda_{\boldsymbol{E_k}} - \lambda_{\boldsymbol{S_k}}\right)\left[2\,\boldsymbol{\beta_k}\boldsymbol{C_{kk}}\boldsymbol{G_k} + \boldsymbol{\beta_k}\sum_{\boldsymbol{i\neq k}}\boldsymbol{C_{ki}}(1-\boldsymbol{\rho_i})\boldsymbol{G_i}\right],$$

$$\boldsymbol{B_k(t)} = 2\,\boldsymbol{C_k^{\rho}}\left[\boldsymbol{S_k} + \boldsymbol{E_k} + \boldsymbol{I_k^A}\right] + \boldsymbol{S_k}(\lambda_{\boldsymbol{Ek}} - \lambda_{\boldsymbol{Sk}})2\,\boldsymbol{\beta_k}\boldsymbol{C_{kk}}\boldsymbol{G_k}$$

$$\text{and } \boldsymbol{\delta_k^*(t)} = \min\left\{0.1, \max\left\{0,\ \frac{\boldsymbol{I_k^A}[\lambda_{\boldsymbol{I_k^A}} - \lambda_{\boldsymbol{Q\ k}}]}{2\boldsymbol{C_T}\boldsymbol{N_k}}\right\}\right\}$$

2.4. Model parameterization

Definition of parameters and baseline values used in the model are shown in Table 1. Data are limited due to unknown times of transitions and the imperfect information on asymptomatic cases. Only the numbers of diagnosed individuals are observed.

3. Results

The controls we investigated were social distancing rates $\boldsymbol{\rho_j(t)}$ and testing rates per day $\boldsymbol{\delta_j(t)}$ in each of the three age groups: children, adults, and seniors humans. We followed a two-stage approach to obtain a numerical solution of the aforementioned controls. First, we simulated a 120-day outbreak period, with an initial condition of one exposed adult ($\boldsymbol{E_a}(0) = 1$) and all others in the susceptible category, in order to calibrate the parameters $\boldsymbol{\beta_j}, \boldsymbol{\gamma}$ as well as the control

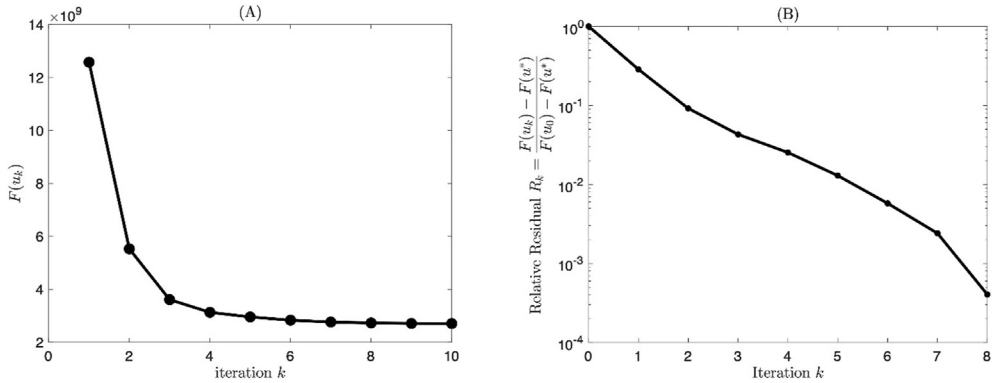

Fig. 3. (A) A plot of the value of the objective function (12) evaluated for each control at iteration $\boldsymbol{k}$, demonstrating monotonic convergence. (B) A plot of the relative residual where we set $\boldsymbol{u^*}$ equal to the control at the iteration that satisfies our convergence criteria as optimal.

parameters $\boldsymbol{\rho_j(t)}$ and $\boldsymbol{\delta_j(t)}$ to create conditions similar to the outbreak conditions reported at the end of June 2020. While our study aimed to determine optimal control strategies, certainly there were some social distancing and testing performed during the 120-day period from February 27, 2020 to June 26, 2020. Therefore, with the simulation and calibration stage, we sought to emulate the parameters and controls during the initial 120-day period, even if not necessarily coordinated to be optimal or consistent. In the simulation we assumed that the reported rates undercount actual cases by a factor of 4 (Fig. 2). For the 120-day period, the social distancing and testing rates were kept constant in time and across age groups. In this simulation the parameters were calibrated to

$$\boldsymbol{\beta_{c,a,s}} = (0.2287,\ 0.0396,\ 0.4994), \quad \gamma = \frac{0.1}{14}$$

$$\boldsymbol{\rho_{c,a,s}} = (0.36, 0.36, 0.36), \quad \boldsymbol{\delta_{c,a,s}} = (0.02, 0.02, 0.02)$$

In the second stage we obtained the optimal control strategy solution for the 180-day period June 26, 2020–December 26, 2020, using the ending condition from the 120-day stage as our initial conditions in this stage. The optimal control strategy was computed numerically using the forward-backward scheme prescribed by Lenhart and Workman (2007) (Lenhart & Workman, 2007). The goal was to minimize the cost function (12) with respect to the six control functions $\boldsymbol{\rho_j(t)}$ and $\boldsymbol{\delta_j(t)}$ for $\boldsymbol{j} \in \{\boldsymbol{c}, \boldsymbol{a}, \boldsymbol{s}\}$. The forward component began with the ending state of the 120-day simulation and an initial guess for the controls, which were chosen to be the control values taken in the 120-day precursor period. The solution to the outbreak model equations (1)–(8) allowed us to solve the reverse time adjoint equation (15) with transversality final conditions (16). At every iteration of the optimal control algorithm, the control iterate is updated by taking a convex combination of the previous control iterate and $\boldsymbol{u_{new}(t)}$, which is computed by solving the optimality condition (17) using the solutions to the adjoint equation. That is $\boldsymbol{u_{new}}$ satisfies $\frac{\partial \boldsymbol{H}}{\partial \boldsymbol{u}}(\boldsymbol{u_{new}}) = 0$. Lenhart and Workman (2007) recommend taking a convex combination of the previous and new controls $\boldsymbol{u_\theta} = (1-\boldsymbol{\theta})\boldsymbol{u_{prev}} + \boldsymbol{\theta}\, \boldsymbol{u_{new}}$ using $\boldsymbol{\theta} = \frac{1}{2}$. However, we found that, for many parameter regimes, this prevented convergence and the algorithm stagnated. To overcome this, we implemented a "greedy" convex combination that evaluates the cost function $\boldsymbol{F}(\boldsymbol{u_\theta}, \mathbf{x_\theta})$, where $\mathbf{x_\theta}$ is the solution to the outbreak model using the controls $\boldsymbol{u_\theta}$ over 100 evenly spaced values of $\boldsymbol{\theta}$ from 0 to 1. Then the new control was selected to minimize the 100 values of the cost function. Thus, the convex combination parameter changed with each forward-backward sweep in a greedy fashion. We found that this approach produced a lesser cost value than when a constant $\boldsymbol{\theta}$ approach converged. Furthermore, by construction, the forward-backward algorithm was monotonically decreasing in the value of the cost function, see Fig. 3. The algorithm was robust in that the same optimal controls were found at convergence when we used the calibrated values of $\boldsymbol{\rho_j}$ and $\boldsymbol{\delta_j}$ as our starting optimal control guesses: $\boldsymbol{u_0} = (\boldsymbol{\rho_j}, \boldsymbol{\delta_j})$ or when we used the minimum or maximum values allowed for the controls as $\boldsymbol{u_0}$.

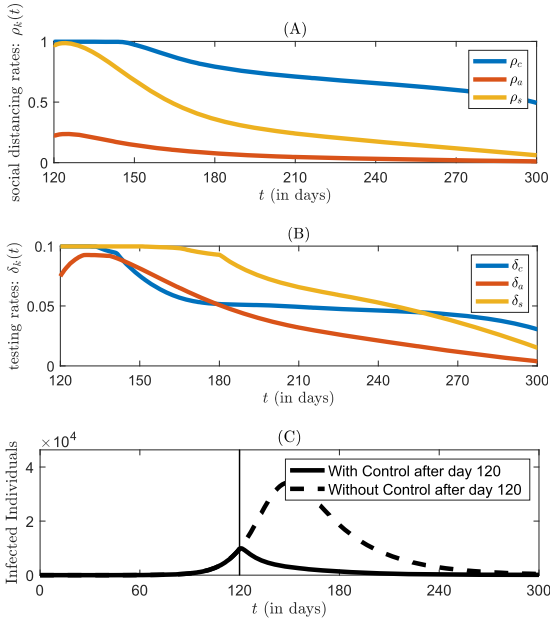

Fig. 4. Optimal control solution for 180-day period for social distancing less than or equal to 100% for the Rio Grande Valley, Texas. (A) Optimal social distancing rates by age group, where $\boldsymbol{\rho_j(t)} \leq 1$. (B) Optimal testing rates by age group, where $\boldsymbol{\delta_j(t)} \leq 0.1$. (C) Total infection incidences with control (solid black line) and without control.

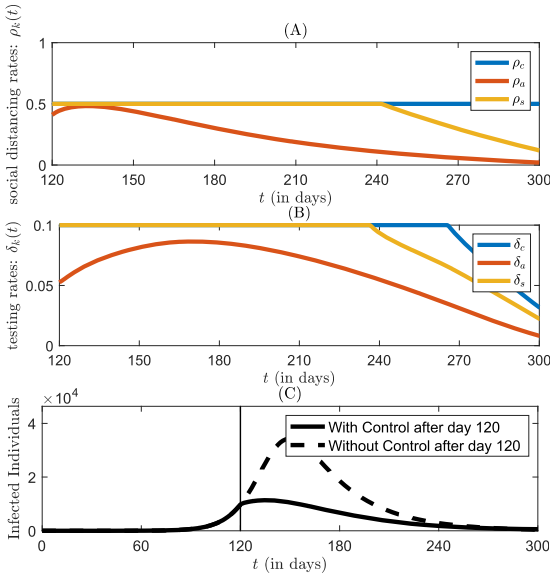

Fig. 5. Optimal control solution for 180-day period for social distancing rates less than or equal to 50% for the Rio Grande Valley, Texas. (A) Optimal social distancing rates by age group, where $\boldsymbol{\rho_j(t) \leq 0.5}$. (B) Optimal testing rates by age group, where $\boldsymbol{\delta_j(t) \leq 0.1}$. (C) Total infection incidences with control (solid line) and without control.

In setting $\boldsymbol{u_{new}}$ to the solution of the optimality condition, $\boldsymbol{u_{new}}$ is a linear combination of the solutions to the reverse time adjoint equation, which were set to zero at the final time in satisfying the transversality condition, and the initial control values. This causes the values of the controls to become zero as $\boldsymbol{t}$ approached the end of the control period. While our experiments showed that choosing the controls optimally can result in infection incidence near zero by the end of the control period, easing social distancing and testing protocols near the end can cause a brief resurgence in the infection. This brief uptick of infections near the end does little to increase the cost function, which is a definite integral over the control period. Indeed, virus resurgences when social distancing mandates have been relaxed have been observed in several cases, including Texas and specifically the RGV (The New York Times, 2020). Therefore, we set our numerical control period to be 20% longer than 180 days, but only took the leading 180 days as our optimal control.

Fig. 4 (A) and (B) depict the optimal social distancing and testing rates, respectively, by age group. That is, these rates minimize the objective function (12), which measures a daily cost or penalty value to social distancing, testing and hospitalization. As the cost to hospitalization is significantly larger than the other costs, we see in Fig. 4(C) that these rates greatly reduce incidences of infection compared to the initial rates. The maximum social distancing rates were set to be 100% and the maximum testing rates per day of the Rio Grande Valley population were set at 10%. The cost of social distancing for both children and seniors were set to be the same, while the cost of social distancing for adults was five times higher. Based on our results, it is feasible to not require extreme social distancing rates for adults, beginning at approximately 25% and decreasing slowly to zero when approaching the end of the 180-day period. However, this requires a very strict testing regime during the first month of the control period and then tapering to a near-constant daily testing rate of 5% for all adults. Fig. 4 shows that children have the highest incidence of infection without control. Children's optimal social distancing was maximal for the first month before a slow taper, but still remained above 50% for the entire control period. The need of a higher than 50% social distancing for children to optimally control incidences of infection was due to the very low value placed on children's social distancing in comparison to adults, as well as due to children's higher contact rates (10)–(11).

To better understand how upper bounds on the control parameters affect the results of our numerical algorithm, we derived optimal social distancing rates when constrained to a maximum rate of 50% (Fig. 5). While the optimal controls prescribed under this regime halt the upward trajectory of infections, the incidence of cases remain nearly constant for about a month before decreasing down. Social distancing rates of adults must begin near the maximum of 50% for approximately a month before decreasing slowly to near zero, as opposed to beginning near 25% and tapering down when social distancing was allowed to reach 100%.

Fig. 6 illustrates an optimal control regime when the daily testing rate was limited to 5%. In this model the optimal social distancing and the infection incidences are similar to those in the model with maximal testing rate of 10%. However, testing rates are near the maximal 5% for both children and seniors, as well as adults for the first half of the control period (Fig. 6).

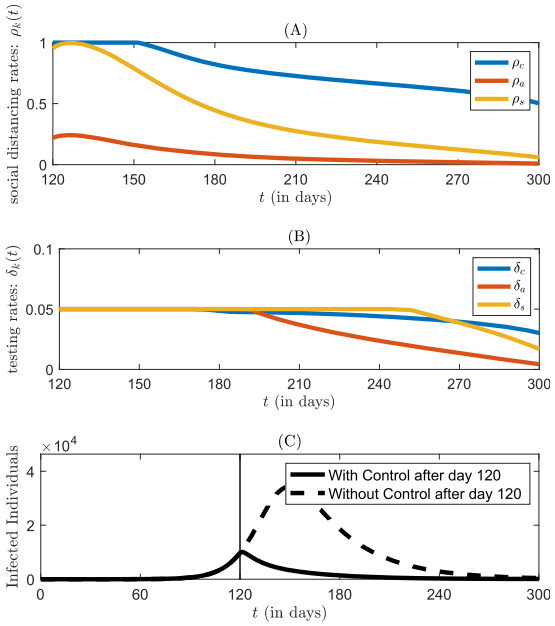

Fig. 6. Optimal control solution for 180-day period at daily testing rate limited to 5% or less for the Rio Grande Valley, Texas. (A) Optimal social distancing rates by age group, where $\boldsymbol{\rho_j(t)} \leq 1$. (B) Optimal testing rates by age group, where $\boldsymbol{\delta_j(t)} \leq 0.05$. (C) Total infection incidences with control (solid line) and without control.

4. Discussion

In this study we found optimal strategies of social distancing and COVID-19 testing to effectively slow the spread of the disease in the RGV. We used optimal control theory in an eight-compartment epidemiological model that depicts COVID-19 transmission. The mathematical framework depicting the dynamics of disease transmission incorporated the time-dependent age-stratified social distancing of susceptible, exposed, and infected asymptomatic cases and testing rates to determine which individuals to isolate. The optimal controls were obtained for 180 days for the period June 26 - December 26, 2020 based on simulated data for a 120-day period from February 27, 2020 to June 26, 2020.

In our numerical experiments, we considered different maximal social distancing (100%, 50%) and testing rates (5%, 10%). Based on our results, control of the spread of the virus involves lessening social distancing between adults by the end of the 180-day period, very strict testing during the first month of the control period and maintaining a constant daily testing rate of 5% followed by isolation of positive cases. We further showed that when the social distancing rate in adults is about 50% and decreases slowly to 25%, both children and seniors should maintain a maximal social distancing rate of 50% for nearly the entire control period, with only the seniors able to ease up in the last two months. This easing of social distancing requires maximal testing rates of children for five of the six months of optimal control and seniors for four of the six months. Adults must also test at higher rates than in the previous scenario. Strict testing at the beginning of the control period and maintaining testing rates are essential to decrease transmission while return-to-work policies are implemented. Testing not only allows officials to isolate the positive cases and therefore limit the spread of disease, but also helps to determine when it is safe to relax restrictions (Guglielmi, 2020).

Studies have evaluated the role of children in spreading virus during influenza season (Huang, Lipsitch, Shaman, & Goldstein, 2014; Worby et al., 2015). The recent reopening of schools in the United States demonstrated that the COVID-19 situation may be similar to what is seen in influenza outbreaks. Within days of starting classes in early August 2020, several clusters of COVID-19 cases emerged in Florida, Georgia, and Mississippi schools (CNN, 2020). Our study supports these early observations. In our model where children play a key role in the spread of the disease given their high contact rates, controlling children's social distancing but not the testing rates is especially crucial to lowering the spread of the infection. Studies conducted in Europe suggested that the infection rate is different in children of different age groups (Edmunds, 2020). Since it is still not clear if there are age-related differences in susceptibility and the likelihood of transmission between children and adolescents, caution should be taken when considering school reopenings. Furthermore, returning to school leads to an increase in work-related contacts in adults (Edmunds, 2020).

Several COVID-19 related studies conducted on different populations used optimal control theory to determine optimal strategies of NPI controls (Perkins & España, 2020; Sasmita, Ikhwan, Suyanto, & Chongsuvivatwong, 2020; Tsay et al., 2020). The majority of these studies modeled the transmission dynamics of COVID-19 using simpler epidemiological compartmental models or used different control variables. Our results agree with prior research that conclude it is possible to achieve relaxation of controls over a period of time (Perkins & España, 2020; Tsay et al., 2020). However, our analysis goes beyond the

reported studies and considers a more complex epidemiological model that accurately incorporates a rapidly evolving understanding of COVID-19 and the likely significant role of pre-symptomatic and asymptomatic transmissions of COVID-19. Moreover, in our study we modeled the transmission of the disease between three age groups in the community and within households and considered the transitions of infected individuals between the different compartments, which is crucial for the culturally unique and high-risk population in the RGV. Lastly, we computed optimal controls in different scenarios, varying the social distancing in each of the age groups and the testing rates in order to suggest school reopenings and return-to-work while controlling and reducing the spread of the virus.

Deterministic epidemiological models are tractable and are standard for making epidemiological inferences, especially when it comes to control measures of the diseases. However, they do not reflect the stochasticity and uncertainty involving the transmission process, especially with a disease like COVID-19. In our case, the compartmental model gave useful insights into optimal control strategies that included qualitative rather than solely quantitative approaches.

In this study we recognize the limitations that the full extent of the current complex and variably effective public health interventions - such as the use of different type face coverings - are not modeled and their impact for this model is uncertain. However, the work by Sasmita et al. (2020) shows that the combination of face mask usage, large-scale social distancing, contact tracing, and case detection and treatment resulted in the optimal strategy to significantly impair viral transmission (Sasmita et al., 2020). The uncertainties regarding the duration of immunity after infection or after vaccination may impact the results of this model over time if and when reinfection or infection is possible in the future. In addition, we did not model the impact of comorbidities and socio-economic statuses in COVID-19 transmission patterns in the RGV. Since transmissibility of the asymptomatic and symptomatic cases remains uncertain (Chen et al., 2020; He et al., 2020; Subramanian, He, & Pascual, 2021), in our study we considered the worst-case scenario that both asymptomatic and mild symptomatic groups are equally infectious. Our conceptual model differs from epidemiological, yet simpler, models proposed by Li et al. (2020) and Lin et al. (2020) to depict early transmission dynamics in Wuhan, China, which assumed a period of zoonotic transmission during December 2019 (Li et al., 2020; Lin et al., 2020) and emigration of a large proportion of population in a short period of time before Wuhan's official lockdown (Lin et al., 2020), both not applicable for the RGV. However, Lin et al. (2020) incorporated in their model's transmission rate all prevention and control measures grouped into two large groups: individual reaction (e.g., contact rate) and governmental action, and demonstrated their need in the model in order to capture the observed pattern (Li et al., 2020). Based on collected epidemiological data from laboratory-confirmed COVID-19 cases in Wuhan, China, the study conducted by Li et al. (2020) supports our findings, recommending considerable efforts in testing for proactive case finding to reduce transmission even in location without local spread yet as well as to permit earlier clinical management of cases (Lin et al., 2020).

Further research of other aspects of the epidemic/pandemic in our region is needed, including the impact of school reopenings, the effectiveness of widespread use of face coverings, the impact of the upcoming flu season, COVID-19 vaccine effectiveness and vaccination rates as well as the extent of vaccination required for optimal herd immunity.

5. Conclusions

Our study suggests that different and lower degrees of social distancing are feasible for adults compared to children. Children have higher contact rates which leads to transmission based on our model, emphasizing the need for caution when considering school reopenings. Over time, as revealed in this model, using similar epidemiological conditions to those of June 26, 2020, after 180 days adults may return to work in limited numbers, which could initially prioritize essential employees followed by those who cannot continue to strive economically in lockdown. This model also highlights that testing and subsequent isolation are crucial and need to continue in order to relax social distancing protocols, and it is possible to drive the infection incidences to zero using a strategy consisting of appropriate social distancing and testing protocols.

Author contributions

KPV lead the study; KPV, TO, and JCM conceived conception and designed the model; TO, JS worked on mathematical model implementation, simulation, and coding; JS and MCV worked on the optimal control modeling and solution; KPV, TO, JS, and JCM contributed to data acquisition; JS, TO and KPV contributed to analysis and interpretation of outputs; KPV, JCM, JS, TO, and MCV worked on the original drafting of the manuscript; KPV, JCM, JS, MCV, TO, and TH revised different drafts of the manuscript; all authors reviewed the final manuscript.

Acknowledgements

We thank Hansapani Rodrigo, Ph.D. in the School of Mathematical & Statistical Sciences, University of Texas Rio Grande Valley, Edinburg, Texas for her assistance in data acquisition.

Appendix

The adjoint equations $\lambda'(t) = -\frac{\partial H}{\partial X_i}$ are explicitly given below for $j \in \{c, a, s\}$, where $\pi_j = \beta_j \sum_{i=c,a,s} [C_{ji}(1-\rho_i)(1-\rho_j) + C_{ji}^H] \frac{(\zeta I_i^A + I_i^M)}{N_i}$ and

$$\frac{d\lambda_{S_j}}{dt} = -\frac{\partial H}{\partial S_j} = -C_j^{\rho}\rho_j^2(t) + \pi_j\lambda_{S_j}(t) - \pi_j\lambda_{E_j}(t)$$

$$\frac{d\lambda_{E_j}}{dt} = -\frac{\partial H}{\partial E_j} = -C_j^{\rho}\rho_j^2(t) + \alpha\lambda_{E_j}(t) - \alpha(1-p)\lambda_{I_j^A}(t) - \alpha p\lambda_{I_j^M}(t)$$

$$\frac{d\lambda_{I_j^A}}{dt} = -\frac{\partial H}{\partial I_j^A} = -C_j^{\rho}\rho_j^2(t) + \mu_A\lambda_{I_j^A}(t) + \delta_j\lambda_{I_j^A}(t) - \delta_j\lambda_{Q_j}(t) + \sum_i \left(\lambda_{S_i}(t) - \lambda_{E_i}(t)\right) S_i\frac{\partial \pi_i}{\partial I_j^A}$$

$$= -C_j^{\rho}\rho_j^2(t) + \mu_A\lambda_{I_j^A}(t) + \delta_j\lambda_{I_j^A}(t) - \delta_j\lambda_{Q_j}(t) + \sum_i \frac{(\lambda_{S_i} - \lambda_{E_i})S_i\beta_i\zeta\left(C_{ij}(1-\rho_j)(1-\rho_i) + C_{ij}^H\right)}{N_j}$$

$$\frac{d\lambda_{I_j^M}}{dt} = -\frac{\partial H}{\partial I_j^M} = (\mu_M + \gamma + q)\lambda_{I_j^M}(t) - \gamma\lambda_{I_j^H}(t) - q\lambda_{Q_j}$$

$$+ \sum_i \frac{(\lambda_{S_i} - \lambda_{E_i})S_i\beta_i\left(C_{ij}(1-\rho_j)(1-\rho_i) + C_{ij}^H\right)}{N_j}$$

$$\frac{d\lambda_{I_j^H}}{dt} = -\frac{\partial H}{\partial I_j^H} = -C_H + (\mu_H + \sigma_j)\lambda_{I_j^H}(t)$$

$$\frac{d\lambda_{Q_j}}{dt} = -\frac{\partial H}{\partial Q_j} = -\nu_Q\lambda_{I_j^H}(t) + (\mu_Q + \nu_Q)\lambda_{Q_j}(t)$$

Declaration of competing interest

The authors declare that they have no known competing financial interests or personal relationships that could have appeared to influence the work reported in this paper.

References

Bolton, K. J., McCaw, J. M., Moss, R., Morris, R. S., Wang, S., Burma, A., et al. (2012). Likely effectiveness of pharmaceutical and non-pharmaceutical interventions for mitigating influenza virus transmission in Mongolia. *Bulletin of the World Health Organization, 90*(4), 264–271. https://doi.org/10.2471/BLT.11.093419

Centers for Disease Control and Prevention. (2021c). Coronavirus disease 2019 (COVID-19). Vaccines. Frequently asked questions about COVID-19 vaccination. https://www.cdc.gov/coronavirus/2019-ncov/vaccines/faq.html. (Accessed 15 March 2021).

Centers for Disease Control and Prevention. (2021a). Coronavirus disease 2019 (COVID-19). *Prevent getting sick*. https://www.cdc.gov/coronavirus/2019-ncov/prevent-getting-sick/index.html. (Accessed 15 March 2021).

Centers for Disease Control and Prevention. (2021b). Coronavirus disease 2019 (COVID-19). People who need extra precautions. People who are at higher risk. https://www.cdc.gov/coronavirus/2019-ncov/need-extra-precautions/groups-at-higher-risk.html. (Accessed 15 March 2021).

Centers for Disease Control and Prevention COVID-19 Response Team. (2020). Severe outcomes among patients with coronavirus disease 2019 (COVID-19) - United States, February 12-March 16, 2020. *MMWR.Morbidity and Mortality Weekly Report, 69*(12), 343–346. https://doi.org/10.15585/mmwr.mm6912e2

Chen, Y., Wang, A., Yi, B., Ding, K., Wang, H., Wang, J., et al. (2020). The epidemiological characteristics of infection in close contacts of COVID-19 in Ningbo city. *Chinese Journal of Epidemiology, 41*. https://doi.org/10.3760/cma.j.cn112338-20200304-00251

Chowell, G., Echevarria-Zuno, S., Viboud, C., Simonsen, L., Tamerius, J., Miller, M. A., et al. (2011). Characterizing the epidemiology of the 2009 influenza A/H1N1 pandemic in Mexico. *PLoS Medicine, 8*(5), Article e1000436. https://doi.org/10.1371/journal.pmed.1000436

CNN. (2020). Some students already started classes. Here's what we have learned so far about America's schools in the pandemic. https://www.cnn.com/2020/08/14/us/schools-reopening-pandemic-lessons/index.html. (Accessed 20 September 2020).

Dong, E., Du, H., & Gardner, L. (2020). An interactive web-based dashboard to track COVID-19 in real time. *The Lancet Infectious Diseases*. https://doi.org/10.1016/S1473-3099(20)30120-1

Edmunds, W. J. (2020). Finding a path to reopen schools during the COVID-19 pandemic. *Lancet Child Adolescent Health*. https://doi.org/10.1016/S2352-4642(20)30249-2

FOX News San Antonio. (2020). Exclusive: Strict shelter-in-place for Rio Grande Valley. https://foxsanantonio.com/news/local/exclusive-strict-shelter-in-place-for-rio-grande-valley. (Accessed 20 September 2020).

Guest, J. L., Del Rio, C., & Sanchez, T. (2020). The three steps needed to end the COVID-19 pandemic: Bold public health leadership, rapid innovations, and courageous political will. *JMIR Public Health and Surveillance, 6*(2), Article e19043. https://publichealth.jmir.org/2020/2/e19043.

Guglielmi, G. (2020). Testing times. https://media.nature.com/original/magazine-assets/d41586-020-02140-8/d41586-020-02140-8.pdf. (Accessed 20 September 2020).

Herrera-Valdez, M. A., Cruz-Aponte, M., & Castillo-Chavez, C. (2011). Multiple outbreaks for the same pandemic: Local transportation and social distancing explain the different "waves" of A-H1N1pdm cases observed in Mexico during 2009. *Mathematical Biosciences and Engineering: MBE, 8*(1), 21–48. http://www.aimspress.com/article/10.3934/mbe.2011.8.21.

He, D., Zhao, S., Lin, Q., Zhuang, Z., Cao, P., Wang, M. H., et al. (2020). The relative transmissibility of asymptomatic COVID-19 infections among close contacts. *International Journal of Infectious Diseases, 94*, 145–147. https://doi.org/10.1016/j.ijid.2020.04.034.

Huang, G., Gong, T., Wang, G., Wang, J., Guo, X., Cai, E., et al. (2020). Timely diagnosis and treatment shorten the time to resolution of coronavirus disease (COVID-19) pneumonia and lowers the highest and last CT scores from sequential chest CT. *AJR.American Journal of Roentgenology, 215*(2), 367–373. https://www.ajronline.org/doi/10.2214/AJR.20.23078.

Huang, K. E., Lipsitch, M., Shaman, J., & Goldstein, E. (2014). The US 2009 A(H1N1) influenza epidemic: Quantifying the impact of school openings on the reproductive number. *Epidemiology, 25*(2), 203–206. https://doi.org/10.1097/EDE.0000000000000055

Kelso, J. K., Milne, G. J., & Kelly, H. (2009). Simulation suggests that rapid activation of social distancing can arrest epidemic development due to a novel strain of influenza. *BMC Public Health, 9*. https://doi.org/10.1186/1471-2458-9-117, 117-2458-9-117.

Kim, S., Kim, Y. J., Peck, K. R., & Jung, E. (2020). School opening delay effect on transmission dynamics of coronavirus disease 2019 in Korea: Based on mathematical modeling and simulation study. *Journal of Korean Medical Science, 35*(13), e143. https://doi.org/10.3346/jkms.2020.35.e143

Koo, J. R., Cook, A. R., Park, M., Sun, Y., Sun, H., Lim, J. T., et al. (2020). Interventions to mitigate early spread of SARS-CoV-2 in Singapore: A modelling study. *The Lancet. Infectious Diseases*. https://doi.org/10.1016/S1473-3099(20)30162-6

KVEO-TV. (2020). Daily updates: What we know about COVID-19 cases in the Rio Grande Valley. https://www.valleycentral.com/news/daily-updates-what-we-know-about-covid-19-cases-in-the-rio-grande-valley/. (Accessed 20 September 2020).

Laing, S. T., Smulevitz, B., Vatcheva, K. P., Rahbar, M. H., Reininger, B., McPherson, D. D., et al. (2015). Subclinical atherosclerosis and obesity phenotypes among Mexican Americans. *Journal of the American Heart Association, 4*(3), Article e001540. https://doi.org/10.1161/JAHA.114.001540

Lauer, S. A., Grantz, K. H., Bi, Q., Jones, F. K., Zheng, Q., Meredith, H. R., et al. (2020). The incubation period of coronavirus disease 2019 (COVID-19) from publicly reported confirmed cases: Estimation and application. *Annals of Internal Medicine, 172*(9), 577–582. https://doi.org/10.7326/M20-0504

Lenhart, S., & Workman, J. T. (2007). *Optimal control applied to biological models* (1st ed.). Chapman and Hall/CRC.

Li, Q., Guan, X., Wu, P., Wang, X., Zhow, L., Tong, Y., et al. (2020). Early Transmission dynamics in Wuhan, China, of novel coronavirus-infected pneumonia. *New England Journal of Medicine, 382*(13), 1199–1207. https://doi.org/10.1056/NEJMoa2001316

Linton, N. M., Kobayashi, T., Yang, Y., Hayashi, K., Akhmetzhanov, A. R., Jung, S. M., et al. (2020). Incubation period and other epidemiological characteristics of 2019 novel coronavirus infections with right truncation: A statistical analysis of publicly available case data. *Journal of Clinical Medicine, 9*(2). https://doi.org/10.3390/jcm9020538

Lin, Q., Zhao, S., Gao, D., Lou, D., Yang, S., Musa, S. S., et al. (2020). A conceptual model for the coronavirus disease 2019 (COVID-19) outbreak in Wuhan, China with individual reaction and governmental action. *International Journal of Infectious Duseases, 93*, 211–216. https://doi.org/10.1016/j.ijid.2020.02.058

Nasrullah, M., Breiding, M. J., Smith, W., McCullum, I., Soetebier, K., Liang, J. L., et al. (2012). Response to 2009 pandemic influenza A H1N1 among public schools of Georgia, United States–Fall 2009. *International Journal of Infectious Diseases, 16*(5), 382–390.

NPR. (2021). The corona virus crisis. How is the COVID-19 vaccination campaign going in your state?. https://www.npr.org/sections/health-shots/2021/01/28/960901166/how-is-the-covid-19-vaccination-campaign-going-in-your-state. (Accessed 15 March 2021).

Oran, D. P., & Topol, E. J. (2020). Prevalence of asymptomatic SARS-CoV-2 infection. A narrative review. *Annals of Internal Medicine*. https://doi.org/10.7326/M20-3012

Pan, X., Chen, D., Xia, Y., Wu, X., Li, T., Ou, X., et al. (2020). Asymptomatic cases in a family cluster with SARS-CoV-2 infection. *The Lancet Infectious Diseases*, 30114–30116. https://doi.org/10.1016/S1473-3099(20)30114-6

Pasco, R., Wang, X., Petty, M., Du, Z., Fox, S. J., Pignone, M., et al. (2020). *COVID-19 healthcare demand projections*. Texas: Austin. https://sites.cns.utexas.edu/sites/default/files/cid/files/covid-19_analysis_for_austin_march2020.pdf?m=1585249934. (Accessed 20 September 2020).

Perkins, T. A., & España, G. (2020). Optimal control of the COVID-19 pandemic with non-pharmaceutical interventions. *Bulletin of Mathematical Biology, 82*(9), 118. https://doi.org/10.1007/s11538-020-00795-y, 020-00795-y.

Prem, K., Cook, A. R., & Jit, M. (2017). Projecting social contact matrices in 152 countries using contact surveys and demographic data. *PLoS Computational Biology, 13*(9), Article e1005697, 10.1371/journal.pcbi.1005697" title="https://doi.org/10.1371/journal.pcbi.1005697">.

Sanche, S., Lin, Y. T., Xu, C., Romero-Severson, E., Hengartner, N., & Ke, R. (2020). High contagiousness and rapid spread of severe acute respiratory syndrome coronavirus 2. *Emerging Infectious Diseases, 26*(7). https://doi.org/10.3201/eid2607.200282

Sasmita, N. R., Ikhwan, M., Suyanto, S., & Chongsuvivatwong, V. (2020). Optimal control on a mathematical model to pattern the progression of coronavirus disease 2019 (COVID-19) in Indonesia. *Global Health Research and Policy, 5*, 38-3020-00163-2. eCollection 2020. 10.1186/s41256-020-00163-2" title="https://doi.org/10.1186/s41256-020-00163-2">.

Shim, E. (2013). Optimal strategies of social distancing and vaccination against seasonal influenza. *Mathematical Biosciences and Engineering: MBE, 10*(5–6), 1615–1634. https://doi.org/10.3934/mbe.2013.10.1615

Subramanian, R., He, Q., & Pascual, M. (2021). Quantifying asymptomatic infection and transmission of COVID-19 in New York City using observed cases, serology, and testing capacity. *Proceedings of the National Academy of Sciences of the United States of America, 118*(9), Article e2019716118. https://doi.org/10.1073/pnas.2019716118

Texas Health and Human Services, Texas Department of State Health Services. (2021). Texas case counts COVID-19 coronavirus disease 2019. https://txdshs.maps.arcgis.com/apps/opsdashboard/index.html#/ed483ecd702b4298ab01e8b9cafc8b83. (Accessed 15 March 2021).

The Conversation. (2020). Coronavirus: Why is Germany's fatality rate so low?. https://theconversation.com/coronavirus-why-is-germanys-fatality-rate-so-low-135496. (Accessed 20 September 2020).

The New York Times. (2020a). Infected but feeling fine: The unwitting coronavirus spreaders. https://www.nytimes.com/2020/03/31/health/coronavirus-asymptomatic-transmission.html. (Accessed 20 September 2020).

The New York Times. (2020b). Coronavirus briefing: What happened today. https://www.nytimes.com/2020/06/25/us/coronavirus-florida-texas-california-arizona.html. (Accessed 20 September 2020).

The United States Census Bureau. (2020). QuickFacts. Willacy county, Texas; Starr county, Texas; Hidalgo county, Texas; Cameron county, Texas; Texas. https://www.census.gov/quickfacts/fact/table/willacycountytexas,starrcountytexas,hidalgocountytexas,cameroncountytexas,TX/PST045219. (Accessed 20 September 2020).

The Week. (2020). Coronavirus research. half of Iceland's COVID-19 spreaders may be asymptomatic, early data suggest. https://theweek.com/speedreads/906119/half-icelands-covid19-spreaders-may-asymptomatic-early-data-suggest. (Accessed 20 September 2020).

Tong, Z. D., Tang, A., Li, K. F., Li, P., Wang, H. L., Yi, J. P., et al. (2020). Potential presymptomatic transmission of SARS-CoV-2, Zhejiang province, China, 2020. *Emerging Infectious Diseases, 26*(5). https://doi.org/10.3201/eid2605.200198

Tsay, C., Lejarza, F., Stadtherr, M. A., & Baldea, M. (2020). Modeling, state estimation, and optimal control for the US COVID-19 outbreak. *Scientific Reports, 10*(1). https://doi.org/10.1038/s41598-020-67459-8

Vatcheva, K. P., Fisher-Hoch, S. P., Reininger, B. M., & McCormick, J. B. (2020). Sex and age differences in prevalence and risk factors for prediabetes in Mexican Americans. *Diabetes Research and Clinical Practice, 159*, 107950. https://doi.org/10.1016/j.diabres.2019.107950 0168-8227

Wan, K., Chen, J., Lu, C., Dong, L., Wu, Z., & Zhang, L. (2020). When will the battle against novel coronavirus end in Wuhan: A SEIR modeling analysis. *Journal of Global Health, 10*(1), Article 011002. https://doi.org/10.7189/jogh.10.011002

Weissman, G. E., Crane-Droesch, A., Chivers, C., Luong, T., Hanish, A., Levy, M. Z., et al. (2020). Locally informed simulation to predict hospital capacity needs during the COVID-19 pandemic. *Annals of Internal Medicine*. https://doi.org/10.7326/M20-1260

Worby, C. J., Chaves, S. S., Wallinga, J., Lipsitch, M., Finelli, L., & Goldstein, E. (2015). On the relative role of different age groups in influenza epidemics. *Epidemics, 13*, 10–16. https://doi.org/10.1016/j.epidem.2015.04.003

World Health Organization. (2020). *Coronavirus disease 2019 (COVID-19) situation report–34*. Geneva, Switzerland: World Health Organization. https://www.who.int/dg/speeches/detail/who-director-general-s-opening-remarks-at-the-media-briefing-on-covid-19–11-march-2020. (Accessed 20 September 2020).

World Health Organization. (2020a). WHO announces COVID-19 outbreak a pandemic. http://www.euro.who.int/en/health-topics/health-emergencies/coronavirus-covid-19/news/news/2020/3/who-announces-covid-19-outbreak-a-pandemic. (Accessed 20 September 2020).

World Health Organization. (2020b). Coronavirus disease (COVID-2019) situation reports. https://www.who.int/emergencies/diseases/novel-coronavirus-2019/situation-reports. (Accessed 15 March 2021).

World Health Organization. (2020c). Report of the WHO-China joint mission on coronavirus disease 2019 (COVID-19). https://www.who.int/publications/i/item/report-of-the-who-china-joint-mission-on-coronavirus-disease-2019-(covid-19. (Accessed 20 September 2020).

Yuan, J., Li, M., Lv, G., & Lu, Z. K. (2020). Monitoring transmissibility and mortality of COVID-19 in Europe. In *International journal of infectious diseases: Ijid*. Official Publication of the International Society for Infectious Diseases. https://doi.org/10.1016/j.ijid.2020.03.050.